Research Square

Preprints are preliminary reports that have not undergone peer review.
They should not be considered conclusive, used to inform clinical practice,
or referenced by the media as validated information.

Study on Flame Retardancy and Smoke Suppression of Silicone Rubber Foam Containing Aluminum Hydroxide and Carbon Molecular Sieve

Furu Kang

kangfuru@xust.edu.cn

Zibo Tian
Jun Deng
Xin Yi
Kai Wang
Xiangliang Tian
Congmeng Hao
Lin Li
Shuaijing Ren
Zujin Bai
Chunhui Lv
Yuchen Liu
Jingxiao Pan
Yushan Hao

Research Article

Keywords: Silicone rubber foam, Carbon molecular sieve, Aluminum hydroxide, Flame retardancy and smoke suppression

Posted Date: August 23rd, 2026

DOI: https://doi.org/10.21203/rs.3.rs-10596398/v1

License: This work is licensed under a Creative Commons Attribution 4.0 International License.
Read Full License

Additional Declarations: No competing interests reported.

Study on Flame Retardancy and Smoke Suppression of Silicone Rubber Foam Containing Aluminum Hydroxide and Carbon Molecular Sieve

Furu Kang[1,2*], Zibo Tian[1], Jun Deng[1,2*], Xin Yi[1,2], Kai Wang[1,2], Xiangliang Tian[4], Congmeng Hao[4], Lin Li[3], Shuaijing Ren[1,2], Zujin Bai[1,2], Chunhui Lv[1,2], Yuchen Liu[1], Jingxiao Pan[1], Yushan Hao[1]

[1] College of Safety Science and Engineering, Xi'an University of Science and Technology, Xi'an 710054, P.R. China.

[2] Shaanxi Key Laboratory of Prevention and Control of Coal Fire, Xi'an University of Science and Technology, Xi'an 710054, P. R. China.

[3] School of Safety Science and Engineering, Henan Polytechnic University, Jiaozuo, Henan 454000, China.

[4] National Mine Safety Technology Innovation CenterBeijing 100083,China.

✉ kangfuru@xust.edu.cn (Furu Kang); dengj518@xust.edu.cn (Jun Deng)

Abstract: To enhance the flame retardancy and smoke suppression performance of silicone rubber foam (SRF), an efficient and environmentally friendly flame-retardant and smoke-suppression system was developed by incorporating aluminum hydroxide ($Al(OH)_3$) and carbon molecular sieve (CMS). $Al(OH)_3$/CMS/SRF composites were fabricated via physical blending, and their flame retardancy, smoke suppression performance, and associated mechanisms were systematically investigated. Results indicate that at mass fractions of 5 wt% and 2 wt% for $Al(OH)_3$ and CMS, respectively, the composite achieves a limiting oxygen index of 30.8% and attains a UL-94 V-0 rating. Compared with pure SRF, the composite exhibits reductions by 21.41%, 51.8%, 70.3%, and 93.9% in peak heat release rate, total heat release, smoke production rate, and total smoke production, respectively, demonstrating excellent flame retardancy and smoke suppression performance at this optimal loading. Mechanistic analysis reveals that CMS provides a physical supporting skeleton and synergistically forms a dense SiO_2/char barrier layer with Al_2O_3, which effectively prolongs the ignition time and

impedes heat and oxygen transfer. This design offers a green, highly efficient synergistic flame-retardant and smoke-suppression strategy, showing great potential for application in silicone rubber foams.

Keywords: Silicone rubber foam; Carbon molecular sieve; Aluminum hydroxide; Flame retardancy and smoke suppression

1 Introduction

Silicone rubber foam (SRF) has attracted widespread attention in building sealing, electronic packaging, and special protection due to its unique elasticity and heat resistance [1-4]. However, the flammability of pure SRF severely restricts its application in scenarios requiring high fire safety. Therefore, improving its flame retardancy has become a research focus [5-7]. To meet practical requirements, modification approaches such as the introduction of flame retardants should be adopted to improve flame retardancy while simultaneously optimizing smoke suppression performance [8-11].

Metal hydroxide flame retardants are widely used due to their strong heat absorption capacity, low smoke release, and environmental friendliness [12-15]. Du et al. [16] introduced 1 wt% ZnNiAl-LDH into SRF, achieving an LOI of 28.6% and a UL-94 V-0 rating, while significantly improving the tensile strength and other mechanical properties. Deng et al. [17] synergistically introduced 0.6 wt% platinum compound, 15 wt% ultrafine $Al(OH)_3$, and 15 wt% ultrafine $CaCO_3$ into SRF; the LOI increased to 35.2% and a UL-94 V-0 rating was achieved, where the catalytic effect of the platinum compound and the endothermic decomposition of $Al(OH)_3$ synergistically enhanced the compactness and stability of the char layer. Kang et al. [18] synergistically introduced 1.5 wt% CNTs-OH and 7 wt% $Mg(OH)_2$ into SRF; the LOI reached 30.5% and a UL-94 V-0 rating was achieved, while the compactness and stability of the char layer were significantly improved. Metal hydroxide flame

retardants have attracted considerable attention owing to their excellent thermal stability, fire performance, and low environmental impact [19-22].

Porous carbon materials significantly enhance the thermal stability and flame retardancy of silicone rubber foam [23-26]. Carbon nanotubes (CNTs) possess excellent thermal, electrical, and mechanical properties [27-29]. Shi et al. [30] introduced 2.0 wt% zinc hydroxystannate/CNT hybrid material into epoxy resin, which reduced the peak heat release rate by 34.2% and effectively inhibited the production of smoke and toxic gases, mainly due to the catalytic synergistic effect of the CNT network and metal compound. Hu et al. [31] constructed PP/APP/CNT composites; the CNT network endowed the composites with an electromagnetic shielding effectiveness of 32.1 dB while simultaneously achieving a UL-94 V-0 rating, realizing the synchronous enhancement of flame retardancy and electromagnetic shielding performance. Compared with carbon nanotubes, carbon molecular sieve (CMS) exhibits unique advantages in gas-phase flame retardancy and thermal insulation; its well-ordered ultra-microporous structure can strongly adsorb combustible small-molecule gases generated by pyrolysis, diluting their concentration and delaying the combustion limit[32-34]. Meanwhile, its extremely large specific surface area enables it to serve as an efficient carrier for uniform dispersion and controlled release of flame retardant components, thereby enhancing the flame retardancy efficiency and synergistic effect of the composites [35-37]. Moreover, CMS can be prepared from a wide range of raw materials, such as lignocellulosic biomass, through mature processes including pyrolysis and activation. This production route is more economical and scalable, which provides an important basis for its application in flame-retardant composites [38-41].

To fill the research gap regarding the synergistic effect between $Al(OH)_3$ and CMS in SRF, a series of $Al(OH)_3$/CMS/SRF composite foams were prepared. A systematic evaluation of the combustion characteristics and smoke release behavior was conducted using limiting oxygen index

(LOI), smoke density testing, and cone calorimetry. The flame retardancy and smoke suppression mechanism of the composite system was further elucidated via FTIR, XPS, SEM, and TG-DTG analyses from the synergistic perspective of condensed-phase char formation enhancement and gas-phase dilution and barrier effects. This study not only filled the research gap regarding the synergistic flame-retardant mechanism between $Al(OH)_3$ and ultra-microporous CMS in SRF, but also revealed the multiphase synergistic effect. The physical adsorption and thermal insulation functions of CMS, combined with the endothermic decomposition of $Al(OH)_3$, constructed a dual protective network of "gas-phase dilution and condensed-phase char formation", which significantly improved the structural stability and smoke suppression performance of SRF under extreme fire conditions.

2 Experimental section

2.1 Material

Cyclic dimethylpolysiloxane (viscosity: 120,000 mPa·s) was purchased from Dongguan Jianuo New Materials Co., Ltd. α,ω-Dihydroxypolydimethylsiloxane with viscosities of 1500 mPa·s and 20–30 mPa·s was supplied by Jiangsu Naen New Materials Co., Ltd. Hydrogen-containing silicone oil (analytical grade) was obtained from Xi'an Daosheng Chemical Technology Co., Ltd. Platinum catalyst (3000 ppm) was provided by Shenzhen Ousibang New Materials Co., Ltd. 2-Methyl-3-butyn-2-ol (analytical grade) was supplied by Shaoguan Keya Fine Chemical Co., Ltd. Nanoscale metal hydroxides, including $Fe(OH)_3$ (200 nm), $Cu(OH)_2$ (200 nm), and $Al(OH)_3$ (300 nm), were all provided by Xi'an Daosheng Chemical Technology Co., Ltd. Carbon-based materials, including carbon molecular sieve (1 mm) and multi-walled carbon nanotubes (10 μm), were obtained from Guangdong Shenghui New Carbon Materials Co., Ltd.

2.2 Sample preparation

To a beaker was added 30 g of cyclic dimethylpolysiloxane (base gum), followed by the

sequential addition of 30 g of α,ω-dihydroxypolydimethylsiloxane with a viscosity of 1500 mPa·s, 1 g of α,ω-dihydroxypolydimethylsiloxane with a viscosity of 20–30 mPa·s, 0.5 g of platinum catalyst, 0.2 g of an inhibitor premixed from α,ω-dihydroxypolydimethylsiloxane (20–30 mPa·s) and 2-methyl-3-butyn-2-ol at a mass ratio of 99:1, and flame retardants with various mass fractions. The mixture was stirred uniformly using a high-speed disperser at 3000 rpm, then 4.3 g of hydrogen-containing silicone oil was quickly added and stirred rapidly for 3–5 min. The mixture was cast into a mold coated with a mold release agent, foamed at room temperature for 4 min, and then dried in an oven at 100 °C for 10 min, thereby obtaining the SRF composite.

2.3 Characterization and testing

The characterization and testing results of the SRF composites are presented in Table 1.

Table 1 Characterization and testing of SRF composites

Instrument	Model	Purpose
Oxygen index analyzer	JF-3	Limiting oxygen index
Horizontal-vertical burning tester	CZF-3	Vertical burning test
Smoke density tester	JCY-2	Smoke production performance
Cone calorimeter	PX07-007	Combustion performance
FTIR	Nicolet iN10	Characterization of residual char functional groups
XPS	K-Alpha	Characterization of residual char elemental composition
SEM	Zeiss GeminiSEM 360	Characterization of residual char morphology and elemental distribution
TG-DSC	Mettler-TGA/DSC-1	Thermal stability

3 Results and discussion

3.1 Screening of flame retardants

To investigate the flame retardancy and smoke suppression performance of single addition of

metal hydroxide/porous carbon material in silicone rubber foam, the limiting oxygen index (LOI), UL-94 rating, maximum smoke density (MSD), and smoke density rating (SDR) were analyzed by varying the loadings of metal hydroxide (1 wt%, 3 wt%, 5 wt%, 7 wt%) and porous carbon material (0.5 wt%, 1 wt%, 1.5 wt%, 2 wt%).

3.1.1 Flame retardancy screening

Figure 1 shows a comparison of the flame retardancy of SRF modified with different modifiers in terms of limiting oxygen index (LOI). In the preliminary screening stage, the LOI of pure SRF sample was only 27.2%, corresponding to a UL-94 V-1 rating. Through the introduction of modifiers, it was found that both metal hydroxides ($Cu(OH)_2$, $Fe(OH)_3$, $Al(OH)_3$) and porous carbon materials (CNTs, CMS) could significantly enhance the flame retardancy of the system. At the optimal loadings, the LOI values of the composites with 5 wt% $Al(OH)_3$ and 2 wt% CMS were increased to 27.8% and 28%, respectively, both achieving a UL-94 V-0 rating without melt dripping. Given $Al(OH)_3$'s excellent smoke suppression potential and CMS's unique ultra-microporous structure, a synergistic flame-retardant system was constructed using these two components to further explore the enhancement mechanism.

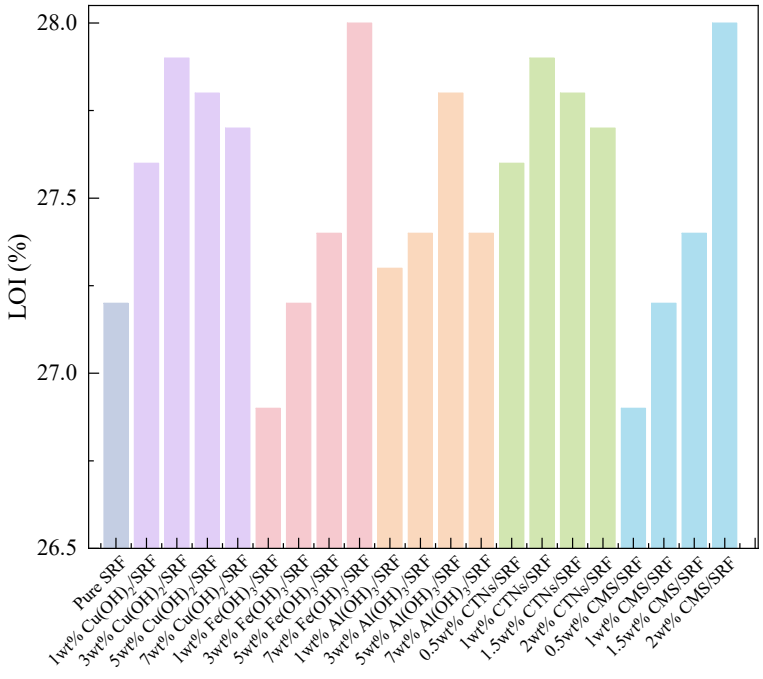


Figure 1. Comparison of LOI of SRF modified with different modifiers

3.1.2 Smoke suppression performance screening

Figure 2 shows a comparison of the smoke suppression performance of SRF modified with different modifiers in terms of smoke density, where the line represents the maximum smoke density (MSD) and the bars represent the smoke density rating (SDR). The MSD and SDR of pure SRF are 49.8% and 30.28%, respectively. Experimental results show that the smoke suppression effect is remarkable after modification with metal hydroxides and carbon materials. Among the metal hydroxide components, $Al(OH)_3$ exhibits the optimal suppression efficiency at a loading of 1 wt%, with reduction rates of both indices exceeding 50%, outperforming $Cu(OH)_2$ and $Fe(OH)_3$. Among the carbon materials, 1 wt% CMS reduces the MSD to 25.49%, outperforming CNTs in smoke density suppression. A comprehensive comparison shows that $Al(OH)_3$ and CMS exhibit the optimal smoke suppression performance in their respective categories, providing an experimental basis for the subsequent construction of a synergistic modification system of the two.

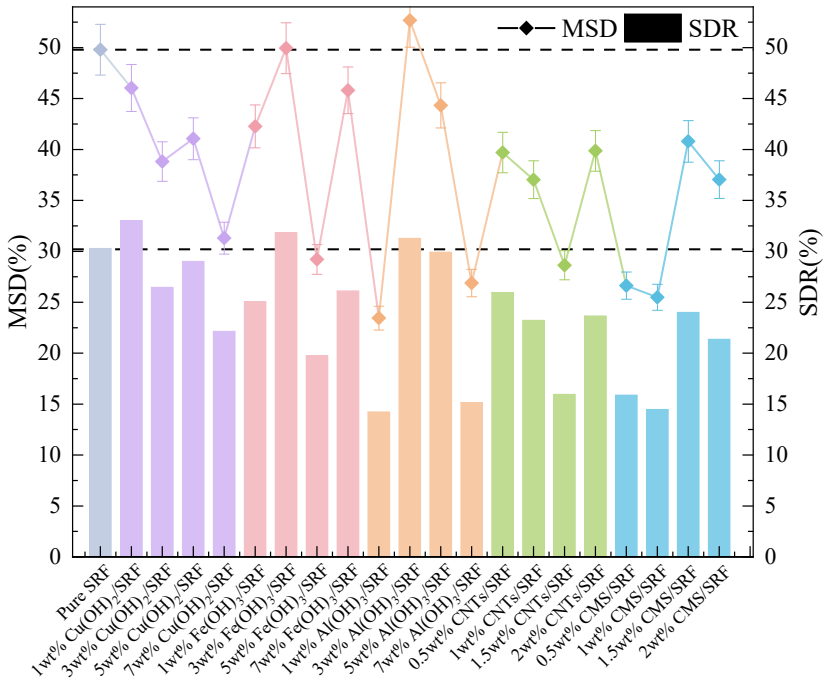


Figure 2. Comparison of MSD and SDR of SRF modified with different modifiers

In summary, based on the comparison in Sections 3.1.1 and 3.1.2, $Al(OH)_3$ and CMS exhibit the most significant effects when separately incorporated into SRF. To systematically investigate the

flame retardancy and smoke suppression performance of SRF with the combined addition of $Al(OH)_3$ and CMS, 20 control groups were designed, and the specific formulations are presented in Table 2.

Table 2 Formulation of $Al(OH)_3$/CMS/SRF composite smoke suppressant

No.	Sample	UL-94	LOI
0	Pure SRF	V-1	27.2
1	1 wt% $Al(OH)_3$/0.5 wt% CMS/SRF	V-0	**29.6**
2	1 wt% $Al(OH)_3$/1 wt% CMS/SRF	V-0	**29.8**
3	1 wt% $Al(OH)_3$/1.5 wt% CMS/SRF	V-0	29.1
4	1 wt% $Al(OH)_3$/2 wt% CMS/SRF	V-0	28.6
5	3 wt% $Al(OH)_3$/0.5 wt% CMS/SRF	V-0	28.2
6	3 wt% $Al(OH)_3$/1 wt% CMS/SRF	V-0	28.6
7	3 wt% $Al(OH)_3$/1.5 wt% CMS/SRF	V-0	**29.5**
8	3 wt% $Al(OH)_3$/2 wt% CMS/SRF	V-0	**29.3**
9	5 wt% $Al(OH)_3$/0.5 wt% CMS/SRF	V-0	28.2
10	5 wt% $Al(OH)_3$/1 wt% CMS/SRF	V-0	28.4
11	5 wt%$Al(OH)_3$/1.5 wt% CMS/SRF	V-0	29.1
12	5 wt%$Al(OH)_3$/2 wt% CMS/SRF	V-0	**30.8**
13	7 wt%$Al(OH)_3$/0.5 wt% CMS/SRF	V-0	28.1
14	7 wt%$Al(OH)_3$/1 wt% CMS/SRF	V-0	**29.2**
15	7 wt%$Al(OH)_3$/1.5 wt% CMS/SRF	V-0	28.3
16	7 wt%$Al(OH)_3$/2 wt% CMS/SRF	V-0	28.1

3.2 Flame retardancy and smoke suppression of $Al(OH)_3$/CMS/SRF composites

3.2.1 LOI and UL-94

The combination of CMS and $Al(OH)_3$ significantly enhances the flame retardancy of the SRF composite, with the corresponding UL-94 test results and LOI data presented in Table 2. As shown in Table 2, when the CMS content is 2 wt% and the $Al(OH)_3$ loading is 5 wt%, the LOI value reaches 30.8%, which is 13.2% higher than that of pure SRF material. Meanwhile, all the combined foam

materials achieve a UL-94 V-0 rating.

3.2.2 MSD and SDR

Figure 3 presents that the MSD and SDR test results of the $Al(OH)_3$/CMS/SRF composite, where the line represents the MSD and the bars represent the SDR. When the $Al(OH)_3$ loading reaches 5 wt% and the CMS loading reaches 2 wt%, the MSD and SDR of the SRF composite are reduced to 21.4% and 13.47%, respectively, showing a reduction of 55.5% and 57.0% compared to those of pure SRF.

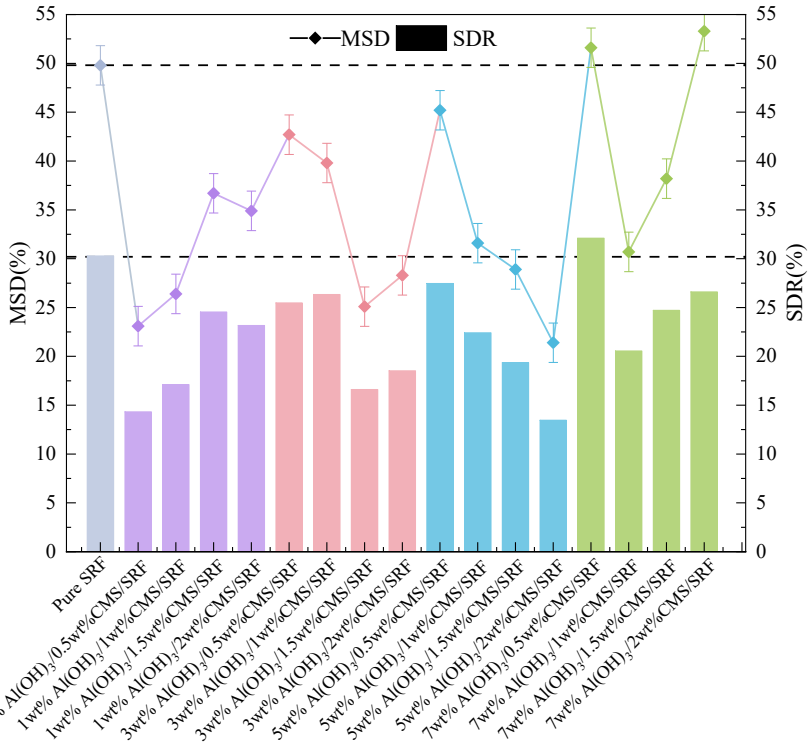


Figure 3. MSD and SDR of $Al(OH)_3$/CMS/SRF

3.2.3 HRR and THR

Based on Sections 3.2.1 and 3.2.2, by leveraging the advantages of the strong endothermic capacity of $Al(OH)_3$ and the large specific surface area of CMS, six groups of optimal composites were selected, in addition to the pristine sample, through the comparison of four key indicators: limiting oxygen index (LOI), UL-94 rating, maximum smoke density (MSD), and smoke density rating (SDR). These seven groups were then subjected to further investigation.

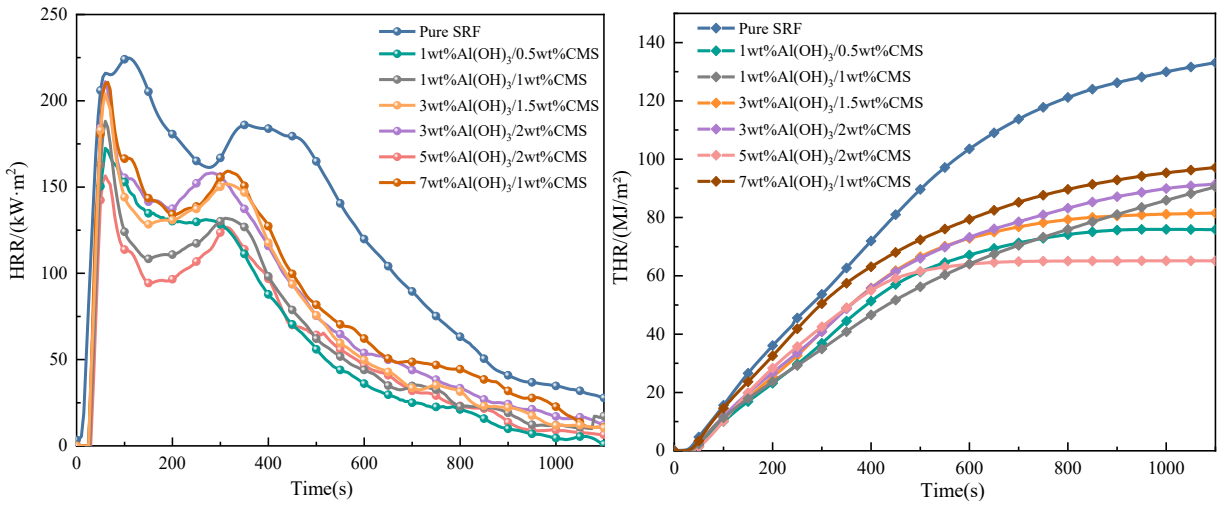


Figure 4. HRR and THR of $Al(OH)_3$/CMS/SRF

Table 3 Summary of heat release data for $Al(OH)_3$/CMS/SRF composites

Sample	TTI (s)	Time to pk_1HRR(s)	pk_1HRR (kW/m^2)	Time to pk_2HRR(s)	pk_2HRR (kW/m^2)	THR (MJ/m^2)
Pure SRF	18	60	215.69	105	225.14	135.25
1 wt% $Al(OH)_3$/0.5 wt%CMS/SRF	25	62	172.50	271	131.12	75.91
1 wt% $Al(OH)_3$/1 wt% CMS/SRF	23	61	188.21	310	131.92	91.19
3 wt% $Al(OH)_3$/1.5 wt% CMS/SRF	22	63	204.20	312	151.92	81.64
3 wt% $Al(OH)_3$/2 wt% CMS/SRF	21	65	211.09	285	158.61	92.22
5 wt% $Al(OH)_3$/2 wt% CMS/SRF	27	66	156.50	310	126.76	65.15
7 wt% $Al(OH)_3$/1 wt% CMS/SRF	20	62	210.73	320	180.97	98.38

As shown in Table 3, the TTI of pure SRF is 18 s. With the introduction of $Al(OH)_3$/CMS, the TTI of the SRF composite is significantly prolonged, increasing by 38.9 %, 27.8 %, 22.2 %, 16.7 %, 50.0 %, and 11.1 %, respectively. This demonstrates that the addition of $Al(OH)_3$/CMS effectively improves the thermal stability and combustion resistance of the material, thereby delaying the ignition time. As shown in Figure 4, after the addition of $Al(OH)_3$/CMS, both the HRR and THR of the SRF composite are significantly reduced. When the $Al(OH)_3$/CMS ratio is increased to 5 wt %/2 wt %, the pk_1HRR reaches 156.50 kW/m^2 at 66 s, and the THR is 65.15 MJ/m^2, which are reduced by 27.4 % and 51.8 %, respectively.

3.2.4 SPR and TSP

Figure 5 shows that as time increases, the SPR of all samples rises rapidly in the initial stage, reaches a peak, and then gradually decreases and stabilizes. Meanwhile, the TSP of pure SRF increases the fastest and eventually attains the highest value, which is consistent with the trend of the SPR. The SPR peak values of the samples with different loadings of $Al(OH)_3$ and CMS are all reduced. In particular, for the sample with 5 wt % $Al(OH)_3$/2 wt % CMS/SRF, the SPR peak value is reduced to 0.00524 m^2/s, with a reduction of 70.3 %, and its TSP is reduced to 0.21277 m^2, showing a reduction of 93.9 %.

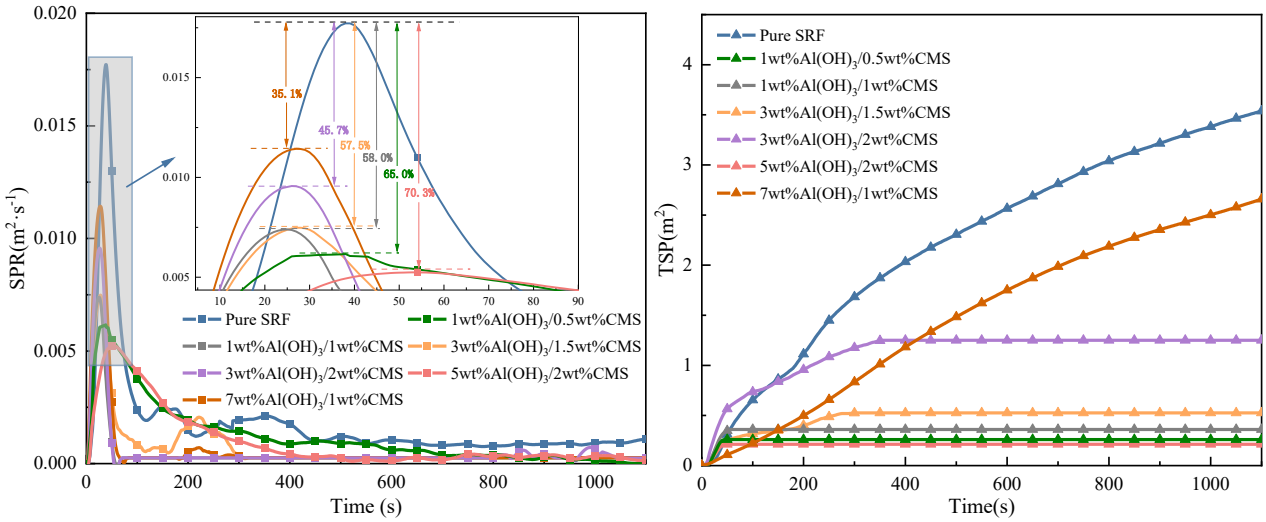


Figure 5. SPR and TSP of $Al(OH)_3$/CMS/SRF

3.3 Char residue analysis of $Al(OH)_3$/ CMS/ SRF composite

3.3.1 Elemental composition analysis of char residue

FTIR analysis of the char residue reveals the regulatory effect of the flame-retardant system on the char-forming mechanism. Figure 6 shows that the characteristic peaks of pure SRF at 3420, 1100, and 1630 cm^{-1} indicate that its char residue is mainly an inorganic SiO_2 framework with some residual Si–C bonds. In contrast, the 5 wt% $Al(OH)_3$/2 wt% CMS/SRF sample exhibits alkyl (–CH_3/–CH_2–) vibration bands at 2973 cm^{-1} and 2830 cm^{-1}, confirming the effective retention of organic components in the char residue. The presence of such organic moieties strongly demonstrates that the synergistic

effect of $Al(OH)_3$ and CMS can significantly suppress the deep pyrolysis of siloxane molecular chains, thereby forming a dense organic–inorganic hybrid char layer. This hybrid structure, by enhancing the mass and heat shielding effect in the condensed phase, constitutes the underlying chemical basis for the excellent flame retardancy and smoke suppression performance of the composite.

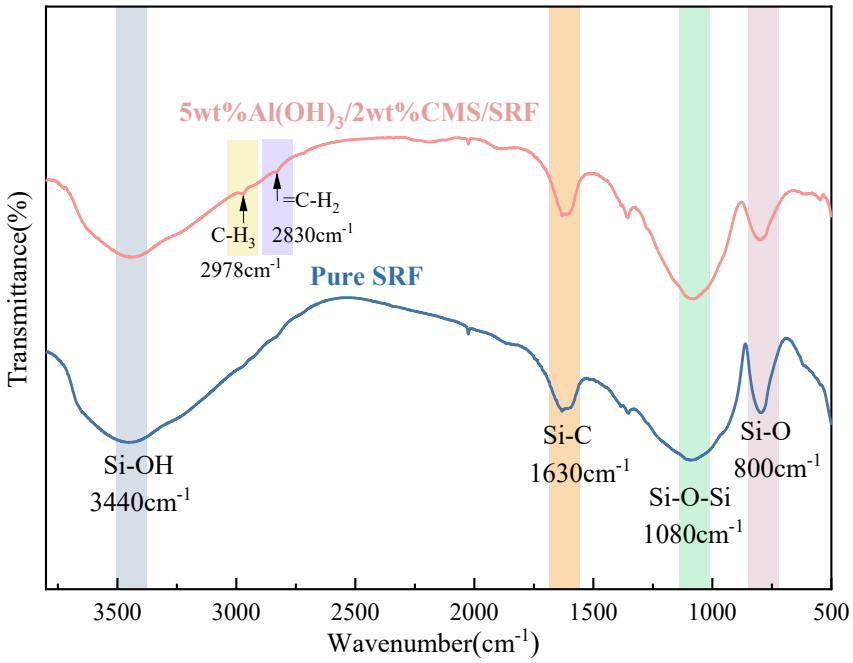


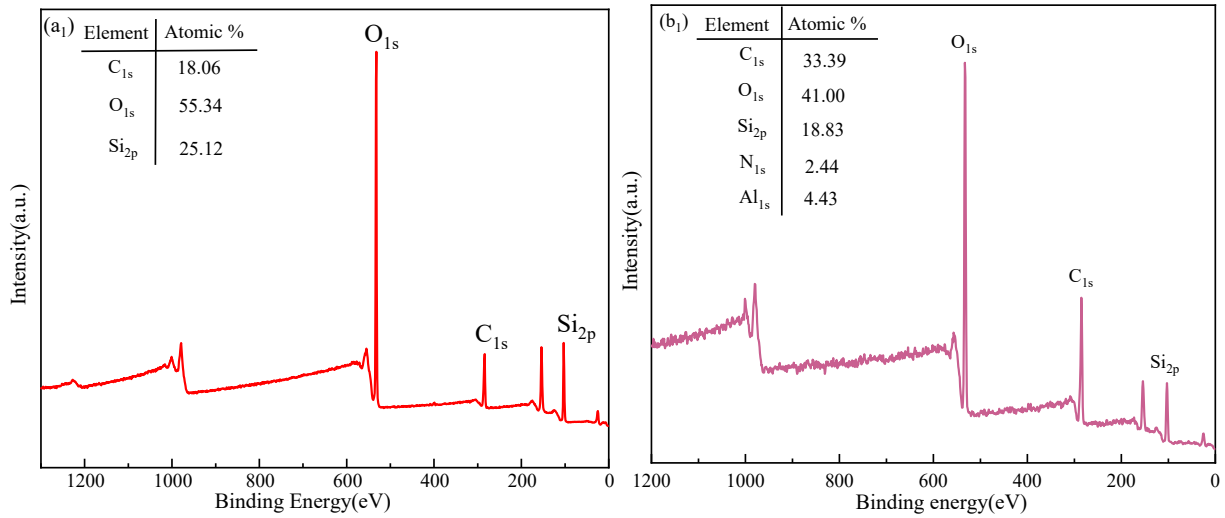
Figure 6. FTIR spectra of char residues from pure SRF and 5 wt% $Al(OH)_3$/2 wt% CMS/SRF composite after combustion.

3.3.2 Elemental composition analysis of char residue

Figure 7 presents the surface elemental composition and content of the char residues after combustion of pure SRF and the 5 wt% $Al(OH)_3$/2 wt% CMS/SRF composite, as detected by XPS, including the full survey spectrum and the peak-fitted high-resolution spectra of C, O, and Si.

Semi-quantitative analysis of the surface elemental composition and chemical state changes of the char residue by XPS reveals the regulatory mechanism of the flame-retardant system on the evolution of the condensed phase. The carbon content in the char residue of pure SRF is only 18.06 at%, while the Si/O atomic ratio is close to 1:2, indicating that the residue is mainly a single SiO_2 inorganic framework. After the introduction of 5 wt% $Al(OH)_3$/2 wt% CMS, the carbon content in the char residue is significantly increased to 33.39 at%, which is attributed not only to the physical

carbon retention effect of CMS but also to the intervention of the flame-retardant system in the oxidation pathway. The C_{1s} peak-fitting results show that the proportion of C=O bonds in the composite increases from 3.12% in pure SRF to 14.53%. This substantial increase in oxygen-containing functional groups suggests that the flame retardant effectively guides the oxidative depolymerization of the molecular chains, leading to the formation of intermediates and a crosslinked char structure with higher thermal stability. Meanwhile, the Si_{2p} spectrum exhibits a remarkably high degree of uniformity, with the proportion of Si–O_2 bonds rising from 84.39% to 93.48%, accompanied by a synchronous increase in the area of the O_{1s} main peak. These features collectively confirm that the synergistic effect of $Al(OH)_3$ and CMS significantly accelerates the conversion of Si into a highly thermodynamically stable silica network and forms a dense organic–inorganic hybrid char layer dominated by C=O and highly crosslinked SiO_2, thereby constructing an efficient physical and thermal barrier.



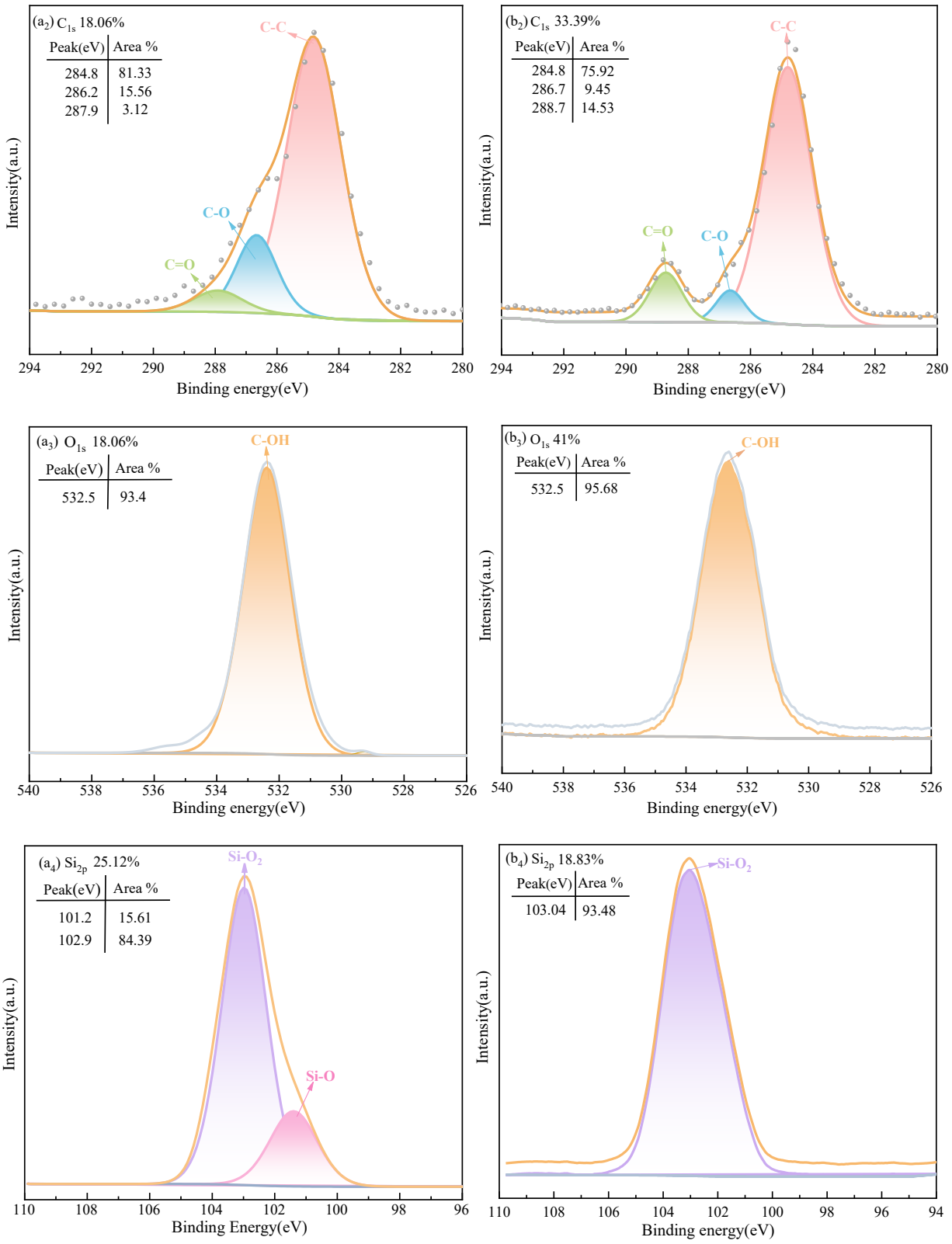


Figure 7. XPS survey spectra of char residues from pure SRF and 5 wt% Al(OH)$_3$/2 wt% CMS/SRF composite, along with peak-fitted high-resolution spectra of C, O, and Si elements.

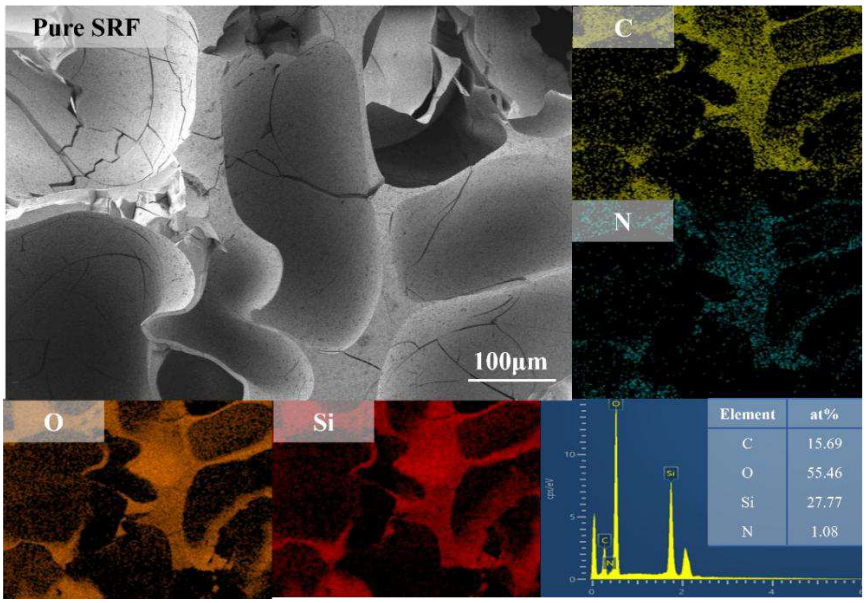
3.3.3 Char residue morphology analysis

Figure 8 presents digital photographs of the char residues from pure SRF and the 5 wt% Al(OH)$_3$/2 wt% CMS/SRF composite after the cone calorimeter test. Since the SRF material is mainly

composed of siloxane polymer, a white SiO_2 deposition layer forms on its surface during combustion, while the structure of the 5 wt% $Al(OH)_3$/2 wt% CMS/SRF composite is more compact.



Figure 8. Photographs of char residues from pure SRF and 5 wt% $Al(OH)_3$/2 wt% CMS/SRF composite after cone calorimeter test.



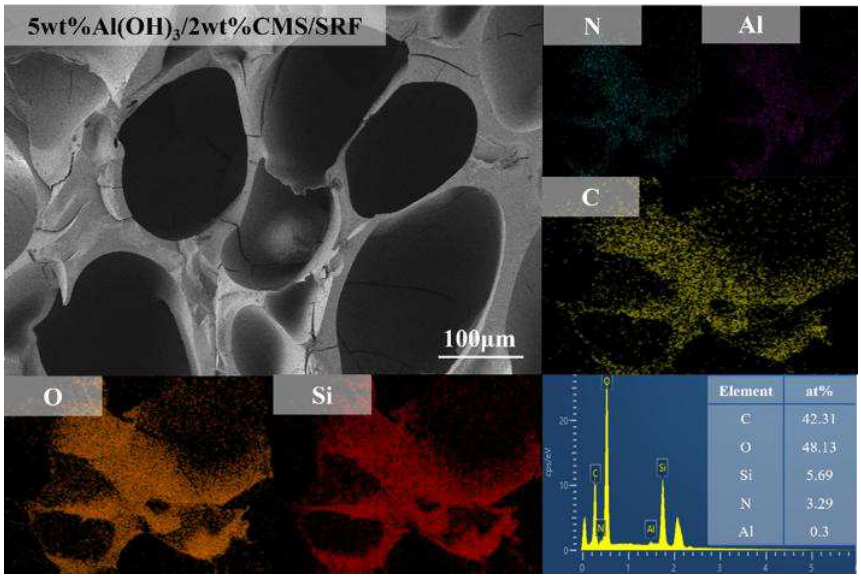
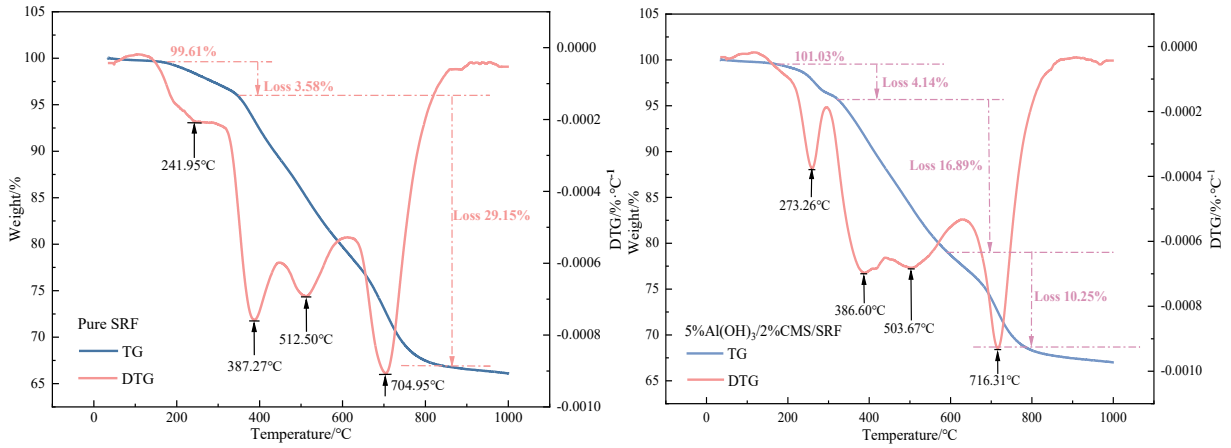


Figure 9. SEM and EDS of pure SRF and 5 wt% $Al(OH)_3$/2 wt% CMS/SRF composite.

SEM analysis of the micro-morphology of the char residue after combustion reveals that the char layer structure of pure SRF is extremely loose and fragmented, with the surface covered by micron-sized cracks. Such a loose architecture is difficult to block the inward and outward transfer of flame and volatile components. EDS results show that the carbon content is only 15.69 at%, and the Si/O atomic ratio is close to 1:2, confirming the substantial loss of organic components and the isolated existence of inorganic SiO_2. In contrast, the char residue of 5 wt% $Al(OH)_3$/2 wt% CMS/SRF exhibits significant structural optimization, the char layer not only displays increased thickness but also forms a dense, continuous and highly intact network. The construction of this dense char layer effectively seals the interior of the material, endowing the composite with a stronger physical barrier effect and manifesting as excellent flame retardancy at the macroscopic level.

3.3.4 TG analysis

To understand the pyrolysis performance of the SRF composite, thermogravimetric analysis was performed. Figure 10 presents the TG and DTG curves of SRF and its composite under a N_2 atmosphere; the specific data are listed in Table 4.



(a)Pure SRF **(b)5 wt% $Al(OH)_3$/2 wt% CMS/SRF**

Figure 10. TG and DTG of Pure SRF and 5 wt% $Al(OH)_3$/2 wt% CMS/SRF

Table 4 TG parameters of SRF composites under N_2 atmosphere

Sample	$T_{-5\%}$(℃)	T_{max}(℃)		Mass loss rate at T_{max}/(%·min^{-1})		Residue (%)
		T_{max1}	T_{max2}	at T_{max1}	at T_{max2}	
Pure SRF	241.95	387.27	704.95	-0.00047	-0.00091	64.55
5 wt% $Al(OH)_3$/2 wt% CMS/SRF	273.26	386.60	716.31	-0.00038	-0.00092	67.03

Note: $T_{-5\%}$ is the initial decomposition temperature; T_{max1} is the temperature at the maximum weight loss rate for the first stage; T_{max2} is the temperature at the maximum weight loss rate for the second stage.

Experimental results show that the introduction of $Al(OH)_3$ and CMS significantly delays the initial degradation of the matrix. The $T_{-5\%}$ of the 5 wt% $Al(OH)_3$/2 wt% CMS/SRF composite is increased from 241.95 °C to 273.26 °C, representing an increase of more than 31.3 °C and demonstrating superior early-stage thermal stability. In the temperature ranges of 313–424 °C and 605–769 °C, the DTG peak pyrolysis temperatures (T_{max1}/T_{max2}) of the composite are higher than those of pure SRF, indicating that the $Al(OH)_3$/CMS system optimizes the condensed phase structure, thereby making the thermal cracking reaction more concentrated and controlled, and effectively retarding the high-temperature decomposition of the siloxane backbone (Si–O–Si). Ultimately, the synergistic system increases the char residue at 900 °C from 64.55% to 67.03%; this increase not only validates the carbon retention effect of the aforementioned hybrid char layer but also provides critical support for the heat shielding and mass transfer barrier of the material at elevated temperatures.

In summary, both $Al(OH)_3$ and CMS can effectively increase the thermal decomposition temperature of SRF and improve its thermal stability. In particular, the combination of 5 wt% $Al(OH)_3$ and 2 wt% CMS exhibits the most significant promoting effect on the catalytic cracking temperature.

3.4 Flame retardant and smoke suppression mechanism of $Al(OH)_3$/CMS/SRF composite

Based on the above analysis, the flame retardant mechanism of the $Al(OH)_3$/CMS/SRF composite can be summarized in Figure 11. At the initial stage of heating, $Al(OH)_3$ undergoes a dehydration reaction, absorbing a large amount of ambient heat and releasing water vapor, which dilutes the combustible gases and oxygen in the gas phase. Meanwhile, the generated Al_2O_3 reconstructs with SiO_2 produced from the thermal decomposition of SRF, forming a dense siliceous protective layer on the material surface. This layer can reflect thermal radiation, block oxygen infiltration, and trap the escaping internal pyrolysis gases and smoke particles. Concurrently, by virtue

of its ultramicroporous structure and catalytic carbonization ability, CMS acts as a physical skeleton within the char residue, transforming the originally loose SRF char layer into a robust, compact, and highly thermally stable intumescent char layer, thereby sealing the mass and heat exchange channels at the gas–solid interface and efficiently adsorbing smoke through its large specific surface area, thus achieving smoke suppression at the source. Consequently, the cooperative construction of a siliceous-carbonaceous dual barrier by the composite components in the condensed phase synergistically optimizes flame retardancy and smoke suppression.

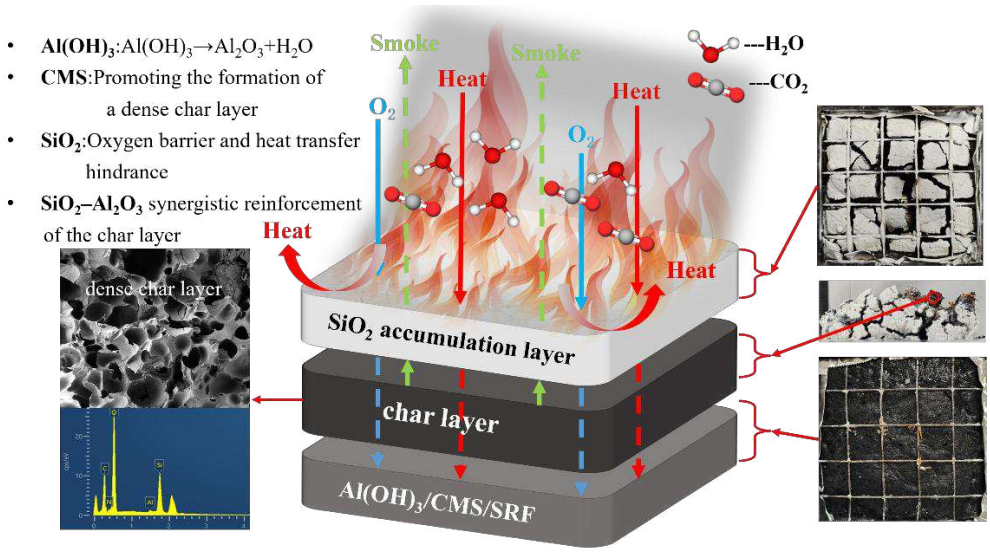


Figure 11. Schematic diagram of the flame retardant and smoke suppression mechanism of the Al(OH)$_3$/CMS/SRF

4. Conclusions

The effects of Al(OH)$_3$ and CMS addition on the flame retardancy and smoke suppression performance of SRF were investigated. The optimal formulation was determined, and the synergistic mechanism was revealed. The main conclusions are as follows:

(1) When Al(OH)$_3$ is added alone, it can effectively improve the flame retardancy of SRF, with 5 wt% being the most ideal addition amount. When CMS is added alone, it can effectively enhance the smoke suppression performance of SRF, with 1 wt% being the most ideal addition amount.

(2) The combined action of Al(OH)$_3$ and CMS can further strengthen the flame retardant and

smoke suppression effects of SRF. When the addition amounts of $Al(OH)_3$ and CMS in SRF are 5 wt% and 2 wt%, respectively, the LOI value reaches 30.8%. Meanwhile, the pkHRR, THR, SPR, and TSP of this material are reduced by 21.41%, 51.8%, 70.3%, and 93.9%, respectively.

(3) The addition of $Al(OH)_3$ and CMS significantly enhances the thermal stability of the composite. The mechanism lies in the synergistic promotion of char layer thickening after SRF combustion, and the effective dilution of combustible gas concentration in the gas phase by the CO_2 released from the reaction.

Declaration of competing interest

The authors declare that they have no known competing financial interests or personal relationships that could have appeared to influence the work reported in this paper.

Data availability

No data was used for the research described in the article.

Acknowledgments

Financial support by Shaanxi Province Youth Innovation Team Project (Grant No.24JP104), Shaanxi Province Innovation Capability Support Program (Grant No.2024RS-CXTD-52) and Science and Technology Nova Plan of Shaanxi Province (Grant No.2023KJXX-048) are gratefully acknowledged.

Funding

Shaanxi Province Youth Innovation Team Project, 24JP104, Furu Kang, Shaanxi Province Innovation Capability Support Program, 2024RS-CXTD-52, Xin Yi, Science and Technology Nova Plan of Shaanxi Province, 2023KJXX-048, Kai Wang

References:

[1] Y Tang, J Liu, Z Chen, Y Li, C Cao, G Zhang, L Tang. Recent advances in fire-retardant silicone Rubber composites. Polymers, 2024, 16(17): 2442. https://doi.org/10.3390/polym16172442

[2] F Kang, J Pan, J Deng, T Zhang, S Ren, L Zhang, C Pan, Y Liu, J Song, J Tu. Synergistic effect of UiO-66-NH_2 and modified steel slag on flame retardancy and smoke suppression of silicone rubber foam. Applied Materials Today, 2025, 47: 102927. https://doi.org/10.1016/j.apmt.2025.102927

[3] X Lou, C Zang, H Pan. Enhancing Flame Retardancy and Thermal Insulation Performance of Silicone Rubber Composites Using Silicon Carbide. Journal of Physics: Conference Series. IOP Publishing, 2024, 2706(1): 012003. https://doi.org/10.1088/1742-6596/2706/1/012003

[4] F Kang, J Song, J Deng, D Wang, R Tian, Z Bai, S Ren, C Su. Synthesis and Fire Suppression Performance of Thermosensitive Microelncapsulated Cis-Hexafluoro-2-Butene. Journal of Vinyl and Additive Technology, 2026. https://doi.org/10.1002/vnl.70075

[5] Q Pang, F Kang, J Deng, L Lei, J Lu, S Shao. Flame retardancy effects between expandable graphite and halloysite nanotubes in silicone rubber foam. RSC advances, 2021, 11(23): 13821-13831. https://doi.org/10.1039/d1ra01409a

[6] AHA Kader, S Dacrory, TA Khattab, S Kamel, H Abou-Yousef. Hydrophobic and flame-retardant foam based on cellulose. Journal of Polymers and the Environment, 2022, 30(6): 2366-2377. https://doi.org/10.1007/s10924-021-02355-4

[7] F Kang, T Zhang, J Deng, L Zhang, Z Bai, J Pan. Effect of Melamine-Modified Zinc Phytate on the Flame Retardancy and Smoke Suppression of Silicone Rubber Foams. Journal of Applied Polymer Science, 2025, 142(24): e57018. https://doi.org/10.1002/app.57018

[8] K Malkappa, C Prasad, CS Kang, SG Jeong, S Sangaraju. Recent developments of phosphorous–

nitrogen-based effective intumescent flame-retardant for polymers and textiles[J]. Polymer Bulletin, 2025, 82(11): 5139-5199. https://doi.org/10.1007/s00289-025-05689-4

[9] A Ishak, C Longuet, B Otazaghine, R Sonnier. Synthesis of novel reactive flame retardant to improve fire resistance and mechanical properties in epoxy resin. Polymer Degradation and Stability,2024. https://doi.org/10.1016/j.polymdegradstab.2024.110925

[10] Y Han, L Yang, Z Yu, Y Zhao, Z Zhang. Lightweight and flame retardant silicone rubber foam prepared by supercritical nitrogen: The influence of flame retardants combined with ceramicizable fillers. Construction and Building Materials, 2023, 370: 130735. https://doi.org/10.1016/j.conbuildmat.2023.130735

[11] F Kang, J Tu, H Zhao, Z Bai, T Zhang. Flame retardancy and smoke suppression of silicone rubber foam with microencapsulated sepiolite and zinc borate. Polymers, 2023, 15(13): 2927. https://doi.org/10.3390/polym15132927

[12] Y Yuan, W Lin, Y Xiao, B Yu, W Wang. Advancements in flame-retardant systems for rigid polyurethane foam. Molecules, 2023, 28(22): 7549. https://doi.org/10.3390/molecules28227549

[13] E Piperopoulos, G Scionti, M Atria, L Calabrese, E Proverbio. Flame-retardant performance evaluation of functional coatings filled with Mg $(OH)_2$ and Al $(OH)_3$. Polymers, 2022, 14(3): 372. https://doi.org/10.3390/polym14030372

[14] T Wu, J Qiu, W Xu, Y Du, W Zhou, H Xie. Efficient fabrication of flame-retarding silicone rubber/hydroxylated boron nitride nanocomposites based on volumetric extensional rheology. Chemical Engineering Journal, 2022, 435: 135154. https://doi.org/10.1016/j.cej.2022.135154

[15] MT Nazir, A Khalid, C Wang, I Kabir, GH Yeoh, BT Phung. Enhancing flame and electrical surface discharge resistance in silicone rubber composite insulation through aluminium hydroxide, clay, and glass fibre additives. Advanced Composites and Hybrid Materials, 2024,

7(2): 57. https://doi.org/10.1007/s42114-024-00874-x

[16] W Du, Z Zhang, H Huang, C Yin. Flame retardancy and mechanical properties of silicone rubber foam composite reinforced with ZnNiAl layered double hydroxides. Journal of Polymer Research, 2023, 30(10): 384. https://doi.org/10.1007/s10965-023-03768-6

[17] J Deng, F Kang, Y Xiao, C Shu, W Wang, L Bin, Z Liu. Effects of platinum compounds/superfine aluminum hydroxide/ultrafine calcium carbonate on the flame retardation and smoke suppression of silicone foams. Journal of Applied Polymer Science, 2020, 137(1): 47679. https://doi.org/10.1002/app.47679

[18] F Kang, J Pan, L Guo, J Deng, D Wang, Z Bai, S Ren, C Su, Pan C, Z Tian. Synergistic Effect of Modified Carbon Nanotubes and Magnesium Hydroxide on Flame Retardancy and Smoke Suppression of Silicone Rubber Foam. Polymer Degradation and Stability, 2025: 111835. https://doi.org/10.1016/j.apmt.2025.102927

[19] J Li, H Zhao, H Liu, J Sun, J Wu. Recent advances in metal-family flame retardants: a review. RSC advances, 2023, 13(33): 22639-22662. https://doi.org/10.1039/d3ra03536k

[20] DK Vo, TD Do, BT Nguyen, CK Tran, TA Nguyen. Effect of metal oxide nanoparticles and aluminum hydroxide on the physicochemical properties and flame-retardant behavior of rigid polyurethane foam. Construction and Building Materials, 2022, 356: 129268. https://doi.org/10.1016/j.conbuildmat.2022.129268

[21] B Guo, P Wang, C Cao, Z Qu, L Lv, G Zhang, Gong L, P Song, J Gao, Y Mai, L Tang. Restricted assembly of ultralow loading of graphene oxide for lightweight, mechanically flexible and flame retardant polydimethylsiloxane foam composites. Composites Part B: Engineering, 2022, 247: 110290. https://doi.org/10.1016/j.compositesb.2022.110290

[22] Q Qu, J Xu, H Wang, Y Yu, Q Dong, X Zhang, Y He. Carbon nanotube-based intumescent flame

retardants achieve high-efficiency flame retardancy and simultaneously avoid mechanical property loss. Polymers, 2023, 15(6): 1406. https://doi.org/10.3390/polym15061406

[23] J Gao, W Huang, W He, L Long, S Qin. Superior flame retardancy of glass fiber-reinforced polyamide 6T composites by synergism between DOPO-based derivative and carbon nanotube. Journal of Thermal Analysis and Calorimetry, 2022, 147(2): 1265-1274. https://doi.org/10.1007/s10973-020-10500-9

[24] A Navidfar, L Trabzon. Recent advances in the multifunctional properties and applications of carbon nanotube/graphene hybrid polymer nanocomposites. Polymer Composites, 2026, 47(1): 29-51. https://doi.org/10.1002/pc.70159

[25] NF Attia. Nanoporous carbon doped with metal oxide microsphere as renewable flame retardant for integrating high flame retardancy and antibacterial properties of thermoplastic polymer composites: NF Attia. Journal of Thermal Analysis and Calorimetry, 2023, 148(12): 5335-5346. https://doi.org/10.1007/s10973-023-12066-8

[26] Y Shi, J Han, A Yao, M Liu, B Wang, C Zhang, H Zou. Constructing SiAPP‐NH2@ MOFs Core‐Shell Structure Toward Hierarchical Composites With Excellent Flame Retardancy, Smoke Suppression, and Electromagnetic Interference Shielding. Journal of Applied Polymer Science, 2025, 142(20): e56898. https://doi.org/10.1002/app.56898

[27] J He, T Fu, S Li, Z Li, J Lu, Y Lin, C Liu, D Guo, W Li, Y Wang. Intumescent closed-cell porous molecular engineering towards high flame retardancy and ultra-low smoke release epoxy resin. Composites Part A: Applied Science and Manufacturing, 2023, 172: 107620. https://doi.org/10.1016/j.compositesa.2023.107620

[28] J Yang, Y Hua, J Zhang, J Sun, H Li, X Gu, S Zhang. Microporous nitrogen-boron compound for epoxy-based composites with improved flame retardancy, toughness, dielectric properties,

transparency, and UV shielding. Composites Part A: Applied Science and Manufacturing, 2025, 197: 109033. https://doi.org/10.1016/j.compositesa.2025.109033

[29] J Liu, R Wang, D Liang, S Zhang, J Feng, M Xu, S Du, B Li. Highly efficient polyethylene composites with flame-retardant, smoke and toxicity suppression properties by incorporating urchin-like ZnO@ CN and intumescent flame retardant. Polymer Degradation and Stability, 2025, 233: 111190. https://doi.org/10.1016/j.polymdegradstab.2025.111190

[30] C Shi, M Wan, X Qian, J Jing, K Zhou. Zinc Hydroxystannate/carbon nanotube hybrids as flame retardant and smoke suppressant for epoxy resins. Molecules, 2023, 28(19): 6820. https://doi.org/10.3390/molecules28196820

[31] Y Hu, D Feng, Y Xie, D Xie. Microwave‐Assisted Confining Flame‐Retardant Polypropylene in Carbon Nanotube Conductive Networks for Improved Electromagnetic Interference Shielding and Flame Retardation. Advanced Engineering Materials, 2021, 23(8): 2100024. https://doi.org/10.1002/adem.202100024

[32] WW Klingler, A Bifulco, C Polisi, Z Huang, S Gaan. Recyclable inherently flame-retardant thermosets: Chemistry, properties and applications. Composites Part B: Engineering, 2023, 258: 110667. https://doi.org/10.1016/j.compositesb.2023.110667

[33] P Lyu, Y Hou, J Hu, Y Liu, L Zhao, C Feng, Y Ma, Q Wang, R Zhang, W Huang, M Ma. Composites filled with metal organic frameworks and their derivatives: recent developments in flame retardants. Polymers, 2022, 14(23): 5279. https://doi.org/10.3390/polym14235279

[34] Z Zheng, H Fan, W Zhang, L Qiao, F Yang, R Yang, W Zhang. Synthesis of crosslinkers based on octa vinyl polyhedral oligomeric silsesquioxane and their flame retardant applications in silicone rubber. Polymer Degradation and Stability, 2025, 238: 111344. https://doi.org/10.1016/j.polymdegradstab.2025.111344

[35] J He, Z Zhang, W Wang, X Guo, Z Zheng. Green Design and Fabrication of a Novel, Bio-based and Multicomponent-Integration Flame Retardant System and Its Application in Improving the Fire Safety of Silicone Rubber. Polymer Degradation and Stability, 2025: 111774. https://doi.org/10.1016/j.polymdegradstab.2025.111774

[36] K Zhu, Y Yang, C Lin, Q Wang, D Ye, H Jiang, K Wu. Effect of compounded aluminum hydroxide flame retardants on the flammability and smoke suppression performance of asphalt binders. ACS omega, 2024, 9(2): 2803-2814. https://doi.org/10.1021/acsomega.3c08094

[37] YH Yoon, D O'Nolan, ML Beauvais, KW Chapman, RP Lively. Direct evidence of the ultramicroporous structure of carbon molecular sieves. Carbon, 2023, 210: 118002. https://doi.org/10.1016/j.carbon.2023.118002

[38] X Ma, N Kang, Y Zhang, Y Min, J Yang, D Ban, W Zhao. Enhancing flame retardancy and smoke suppression in epoxy resin composites with sulfur‐phosphorous reactive flame retardant. Molecules, 2023, 29(1): 227. https://doi.org/10.3390/molecules29010227

[39] Y Shi, L He, D Chen, Q Wang, J Shen, S Guo. Simultaneously improved electromagnetic interference shielding and flame retarding properties of poly (butylene succinate)/thermoplastic polyurethane blends by constructing segregated flame retardants and multi-walled carbon nanotubes double network. Composites Part A: Applied Science and Manufacturing, 2020, 137: 106037. https://doi.org/10.1016/j.compositesa.2020.106037

[40] MR Hasnat, MK Hassan, S Saha. Flame retardant polymer composite and recent inclusion of magnesium hydroxide filler material: A bibliometric analysis towards further study scope. Fire, 2023, 6(5): 180. https://doi.org/10.3390/fire6050180

[41] OO Oghenetega, P Fulvio, NS Bobbitt, KS Walton. Single-Component Adsorption Equilibria of CO_2, CH_4, Water, and Acetone on Tapered Porous Carbon Molecular Sieves. Journal of Chemical

1 & Engineering Data, 2024, 69(3): 1411-1422. https://doi.org/10.1021/acs.jced.3c00368